Multiplex assay for condition-dependent changes in protein–protein interactions

Ulrich Schlecht, Molly Miranda, Sundari Suresh, Ronald W. Davis, and Robert P. St.Onge[1]

Stanford Genome Technology Center, Department of Biochemistry, Stanford University, Palo Alto, CA 94304

Edited by Stanley Fields, Howard Hughes Medical Institute/University of Washington, Seattle, WA, and approved April 17, 2012 (received for review April 3, 2012)

Changes in protein–protein interactions that occur in response to environmental cues are difficult to uncover and have been poorly characterized to date. Here we describe a yeast-based assay that allows many binary protein interactions to be assessed in parallel and under various conditions. This method combines molecular barcoding and tag array technology with the murine dihydrofolate reductase-based protein-fragment complementation assay. A total of 238 protein-fragment complementation assay strains, each representing a unique binary protein complex, were tagged with molecular barcodes, pooled, and then interrogated against a panel of 80 diverse small molecules. Our method successfully identified specific disruption of the Hom3:Fpr1 interaction by the immunosuppressant FK506, illustrating the assay's capacity to identify chemical inhibitors of protein–protein interactions. Among the additional findings was specific cellular depletion of the Dst1:Rbp9 complex by the anthracycline drug doxorubicin, but not by the related drug idarubicin. The assay also revealed chemical-induced accumulation of several binary multidrug transporter complexes that largely paralleled increases in transcript levels. Further assessment of two such interactions (Tpo1:Pdr5 and Snq2:Pdr5) in the presence of 1,246 unique chemical compounds revealed a positive correlation between drug lipophilicity and the drug response in yeast.

protein network | cell-based assay | drug screening | chemogenomics

Protein–protein interactions (PPIs) are of fundamental importance to virtually all cellular processes, including signal transduction and regulation of gene expression. Emergent high-throughput technologies that identify protein complexes and/or binary interactions have produced a wealth of information and have further underscored the ubiquitous role that PPIs play in cell biology (1–8). Although changes in protein complexes can occur from routine biochemical signaling events (i.e., posttranslational modification, protein degradation, or relocalization), the aforementioned studies were performed under standard growth conditions, and thus network connectivity changes that occur in response to different environmental cues remain ill-defined. Measuring such changes—for example, in response to chemical (i.e., small molecule) perturbations—is valuable in understanding both cellular systems and the biological effects of the chemical in question (9).

The cell's "interactome" also represents a tremendous opportunity for unique therapeutic strategies. Small-molecule drugs that directly inhibit specific PPIs could be used to modulate the activity of certain cellular processes while minimally interfering with others. PPIs are perceived to be among the most challenging targets for small molecules because of the sheer size of the interaction interface and the lack of small, deep cavities amenable to small-molecule binding (reviewed in ref. 10). Thus, despite an ever-increasing commitment by drug developers to pursue PPIs, and a growing list of small molecules that can disrupt PPIs, a need exists for new approaches to identifying such inhibitors and better illuminating the druggability of this coveted class of therapeutic targets (11, 12).

The protein-fragment complementation assay (PCA) is an established method for identifying interactions between protein pairs (13). In this assay, two proteins of interest are fused to complementary fragments of a reporter protein, and, upon interaction of the two fusion proteins, the reporter is reconstituted. DNA barcodes, on the other hand, permit multiplexing of biological samples rather than laboriously assaying them one at a time. For example, the incorporation of unique 20mer DNA sequences in the yeast deletion mutant collections enables thousands of individual strains to be assayed simultaneously (14–16). Here we combine the PCA methodology with molecular barcode technology in a multiplex assay to (*i*) identify chemical modulators of PPIs, (*ii*) better understand the dynamic nature of the PPI network, and (*iii*) characterize the mode of action of bioactive chemicals. We have tested the effects of 80 diverse compounds on a set of barcoded PCA strains representing 238 unique binary complexes. Our results validate this approach as an effective method for highly parallel analysis of dynamic PPIs in vivo.

Results

Construction of a Pool of BarCoded PCA Strains. In the murine dihydrofolate reductase-based protein-fragment complementation assay (mDHFR PCA), the interaction of two proteins of interest allows a yeast strain to grow in the presence of the DHFR inhibitor methotrexate (MTX). The assay is based on a mutated version of the murine DHFR enzyme that is insensitive to MTX but has full catalytic activity in yeast (17, 18). This tool has been used to systematically interrogate nearly all possible binary combinations of yeast proteins and has led to the identification of 2,770 PPIs (8). We randomly selected strains representing 384 PPIs from this dataset and tested their ability to grow in liquid media in the presence of MTX (Fig. 1). Approximately 64% of the strains (246 to be exact) were verified to grow under our culture conditions. We also constructed a strain harboring the Hom3:Fpr1 protein pair, an interaction that was not reported in ref. 8 but that was identified in yeast two-hybrid screens (5, 6). Importantly, the interaction between Hom3 and Fpr1 was previously shown to be disrupted by the immunosuppressive drug FK506 (tacrolimus) (19). The Hom3:Fpr1 PCA strain exhibited robust growth under MTX selection, indicating that the PCA system successfully identifies an interaction between the two proteins.

The growth rates of these 247 PCA strains were virtually indistinguishable in the absence of MTX selection (Fig. 2*A*); however, a wide range of growth rates were observed when MTX was present in the media (Fig. 2*B*). Although the precise underlying cause of these growth differences is not completely understood, differences in the absolute number of reconstituted mDHFR complexes per cell is presumably the major factor.

Two unique molecular barcodes (an "UP tag" and a "DOWN tag") were used to determine the abundance of individual strains following competitive (i.e., pooled) growth under MTX selection. Ten replicate pool experiments were performed to assess reproducibility (*SI Materials and Methods*). The raw fluorescence values of the UP tag and DOWN tag for each strain were found

Author contributions: U.S., R.W.D., and R.P.S. designed research; U.S., M.M., and S.S. performed research; U.S. and R.P.S. analyzed data; and U.S. and R.P.S. wrote the paper.

The authors declare no conflict of interest.

This article is a PNAS Direct Submission.

Freely available online through the PNAS open access option.

Data deposition: The microarray data reported in this paper has been deposited in the European Bioinformatics Institute's repository ArrayExpress, http://www.ebi.ac.uk/arrayexpress (accession no. E-MEXP-3467).

[1]To whom correspondence should be addressed. E-mail: bstonge@stanford.edu.

This article contains supporting information online at www.pnas.org/lookup/suppl/doi:10.1073/pnas.1204952109/-/DCSupplemental.

SYSTEMS BIOLOGY

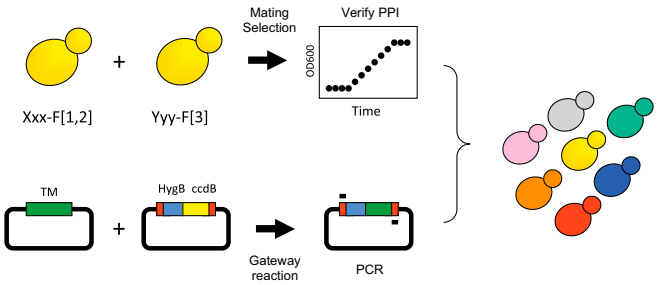

Fig. 1. Construction of a pool of barcoded PCA strains. (*Upper*) Haploid strains expressing PCA proteins of interest (Xxx-F[1,2] or Yyy-F[3]) were mated and diploids were selected. Interaction between Xxx and Yyy was verified in liquid minimal media supplemented with MTX. (*Lower*) Gateway-compatible entry vectors, each containing a unique tag module (TM), were recombined with a destination vector containing the hygromycin B marker (indicated in blue) and the counterselectable *ccdB* marker (indicated in yellow), flanked by *HO* (a gene important for mating-type switching that is transcriptionally repressed in diploids) homology (indicated in red). The resulting vectors were then used as template to PCR-amplify the TM cassette (containing two unique barcodes, an "UP tag" and a "DOWN tag") with flanking regions complementary to the *HO* locus. Integrative transformation was used to create a pool of barcoded PCA strains (depicted by differently colored yeast cells, see *SI Materials and Methods*).

to be well correlated (R = 0.79; Fig. 2*C*), the majority of barcodes (96%) were detected in all samples (Fig. 2*D*), and a pair-wise comparison of the 10 replicates showed a very high correlation (R = 0.98; Fig. 2*E*). We also observed a strong correlation between array hybridization signal following pooled growth and growth rate measured in isogenic cultures (R = 0.88; Fig. 2*F*). Taken together, these data demonstrate that the growth kinetics of many individual PCA strains, and therefore their underlying protein complexes, can be interrogated in a single pooled culture with high reproducibility.

Multiplex Interrogation of Protein–Protein Interactions with Small Molecules. When applied to the PCA pool, chemical compounds that alter the abundance of a specific binary complex will concurrently change the number of reconstituted mDHFR complexes per cell, which will alter the cell's resistance to MTX and thus change the growth rate of that strain relative to others in the pool. In principle, chemicals could elicit these changes directly by disrupting the interaction interface between proteins or indirectly, for example, by altering gene expression and consequently the abundance of either member of the protein complex.

We tested the impact of 80 compounds (Dataset S1) on the 238 strains (those with tag signals above background) in our PCA pool. An interaction score was calculated for all chemical-PPI pairs on the basis of the change in barcode abundance, and thus on the basis of the change in the underlying binary complex, in response to chemical treatment (Dataset S2 and *SI Materials and Methods*). Twelve chemical-PPI pairs with interaction scores < -10 and 42 pairs with interaction scores >10 are highlighted in red and green, respectively (Fig. 3*A*). These 54 pairs and 6 pairs with scores close to zero were retested using isogenic cultures (Dataset S3). Data from the pooled and the single-strain cultures were in good agreement (R = 0.88; Fig. 3*B*), and from these data we assembled a high-confidence list of 46 chemical-induced changes (6 cases of reduced binary complex levels and 40 cases of increased levels) (*SI Materials and Methods* and Dataset S3).

Among the high-confidence chemical-PPI pairs was Hom3:Fpr1 in FK506. The Hom3:Fpr1 strain clearly exhibited the strongest sensitivity to FK506 compared with other strains in the pool (Fig. 3*C*). FK506 treatment also resulted in a specific increase in growth of the Pdr5:Pdr5, Tpo1:Pdr5, and Snq2:Snq2 strains (Fig. 3*C* and discussed further in Fig. 5). We further examined the effects of FK506 on growth of individual strains both in the presence and the absence of MTX (representative growth curves are shown in Fig. S1). Consistent with the multiplex assay, the Hom3:Fpr1 strain was highly sensitive to FK506 relative to a control strain when both were grown under MTX selection (Fig. 3*D*, *Upper Right*). Similarly, the Pdr5:Pdr5, Tpo1:Pdr5, and Snq2:Snq2 strains were confirmed to grow significantly faster in response to FK506 (Fig. 3*D*, *Lower Right*). Importantly, these strain-specific FK506-induced growth changes were entirely dependent on MTX selection and were not observed when strains were grown in the absence of MTX (Fig. 3*D*, *Left* panels). Collectively, these results are consistent with FK506-dependent reduction in the cellular abundance of the Hom3:Fpr1 complex and with increase in the Pdr5:Pdr5, Tpo1:Pdr5, and Snq2:Snq2 complexes. More broadly, given that FK506 is known to disrupt the Hom3:Fpr1 interaction directly (19), our results indicate that mDHFR–PCA interactions are reversible in vivo and thus amenable to identifying chemical inhibitors of PPIs. In addition, they demonstrate that loss (or gain) of a single PPI can be readily detected with our multiplex assay.

Specific Depletion of the Dst1:Rbp9 Complex by Doxorubicin in Vivo. We observed that growth of the Dst1:Rpb9 strain was specifically

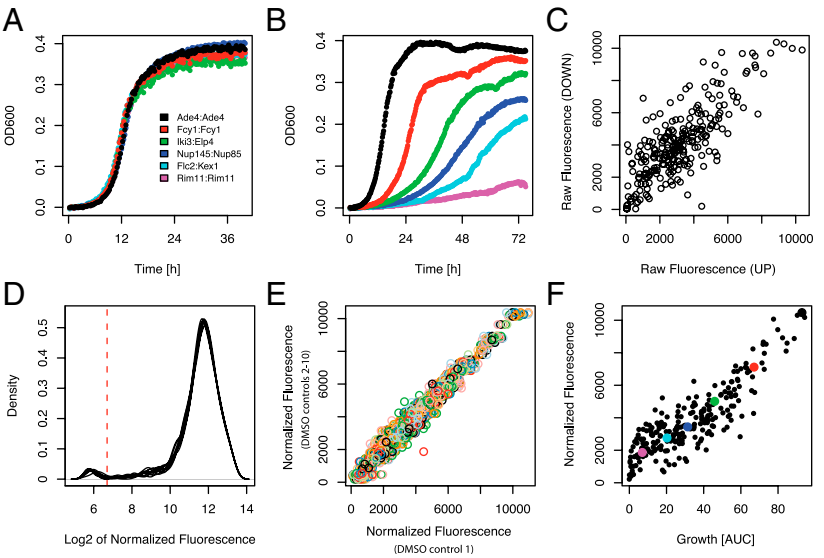

Fig. 2. Characterization of the PCA pool. (*A*) Superimposed growth curves of isogenic cultures of six PCA strains (*Inset*). Strains were grown in minimal media in the absence of MTX, and optical density (OD_{600}, *y* axis) of the culture was measured every 15 min for 36 h (*x* axis). (*B*) As in *A*, but minimal media was supplemented with 100 μg/mL MTX and growth was followed for 72 h. (*C*) Scatterplot comparing the raw fluorescence values of the UP tag (*x* axis) and DOWN tag (*y* axis) for each strain in the pool following growth under MTX selection. Values were averaged from 10 replicate experiments. (*D*) Density plot depicting the distribution of barcode fluorescence (quantile normalized and log2-transformed) in the 10 replicate experiments. The red dashed line indicates 100 fluorescence units (more than twice the median fluorescence of unused features on the array). (*E*) Scatterplot comparing the quantile normalized barcode fluorescence values measured in the 10 replicate experiments. One replicate was used as a reference (*x* axis), and the remaining nine replicates (each represented by a different color on the *y* axis) were plotted against this reference. (*F*) Scatterplot comparing the fluorescence value of each strain on the array [averaged from 10 replicates and UP and DOWN tags (*y* axis)] to the growth rate in isogenic culture (see *SI Materials and Methods* for description of *x* axis). Strains represented in *A* and *B* are indicated by large colored circles. Color scheme as in *A*.

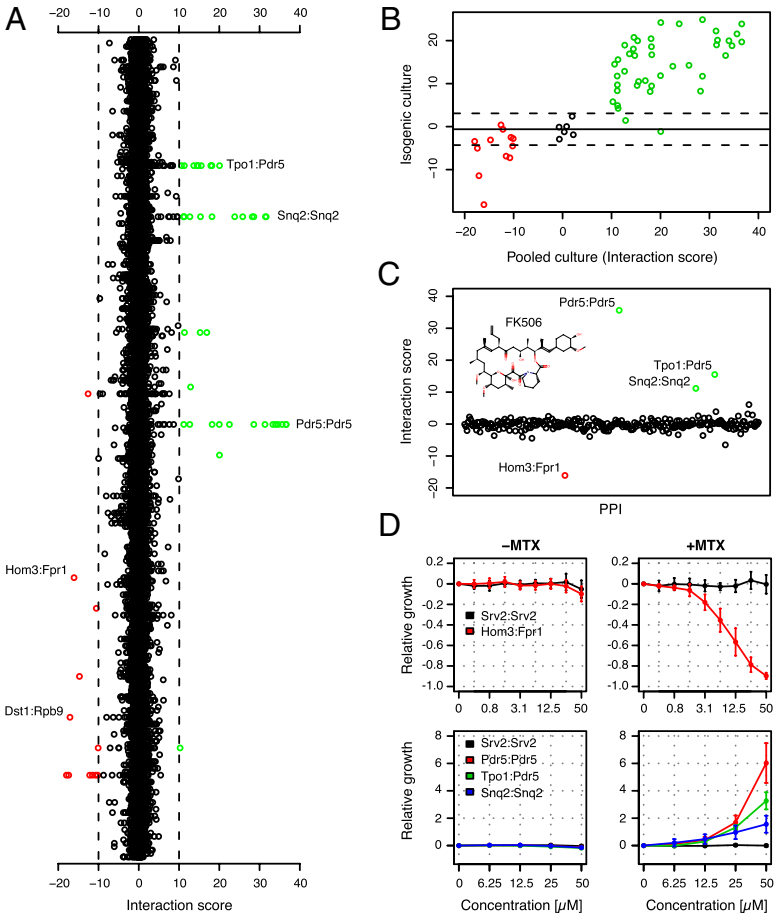

Fig. 3. Chemical screening of the PCA pool. (*A*) Eighty compounds were screened against the pool, and interaction scores were calculated for every chemical-PPI combination (*SI Materials and Methods*). The scatterplot depicts the 80 interaction scores (plotted on the *x* axis) for each of the 238 PCA strains (arranged on the *y* axis). Chemical-PPI pairs with an interaction score less than −10 are marked in red, and those with an interaction score greater than 10 are marked in green. (*B*) The 54 chemical-PPI pairs indicated in red and green in *A*, plus 6 pairs with interaction scores near zero (controls), were assayed in isogenic cultures (*SI Materials and Methods*). Chemical-induced changes in growth rate are plotted on the *y* axis and the interaction scores determined in the pool experiment on the *x* axis. The solid line indicates the mean of the six controls, and the dashed lines mark two SDs above and below the mean. (*C*) Dot plot depicting interaction scores of 238 PPIs (arranged alphabetically on the *x* axis) assayed in 50 μM FK506. PPIs that fell below or above the thresholds in *A* are labeled and indicated in red and green, respectively. The chemical structure of FK506 is shown. (*D*) Confirmation of pool data with isogenic cultures. Individual strains (*Inset*) were grown in the presence (*Right* panels) or absence (*Left* panels) of MTX in increasing concentrations of FK506 (concentrations are indicated on the *x* axis of each plot). Growth relative to that in the absence of FK506 is indicated by the *y* axis and was calculated as follows: Relative growth = $(AUC_{FK506} - AUC_{DMSO})/AUC_{DMSO}$ (*SI Materials and Methods*). The mean of three replicates are plotted, and error bars represent the SD.

inhibited by the anthracycline drug doxorubicin in our multiplex assay (Fig. 4*A*). Rpb9 is a subunit of RNA polymerase II, and Dst1 is a general transcription elongation factor for RNA polymerase II that enables elongation through transcription arrest sites (20, 21). Doxorubicin (adriamycin) is used to treat cancer and is thought to work primarily by intercalating DNA and inhibiting the progression of topoisomerase II (22, 23). In yeast, Ssl2, a DNA-dependent helicase, has been identified as a potential target of doxorubicin (24, 25). As a member of the RNA polymerase transcription factor TFIIH complex, Ssl2 is thought to have dual roles in nucleotide excision repair and transcription (26, 27). Thus, doxorubicin-dependent decrease of Dst1:Rpb9 complex levels further supports an emerging, yet enigmatic, mechanism for doxorubicin involving transcription.

We explored this result further by testing the effects of doxorubicin and three related anthracycline drugs (daunorubicin, epirubicin, and idarubicin) on the Dst1:Rpb9 strain in isogenic cultures (Fig. 4*B*). Under MTX selection, doxorubicin, daunorubicin, and epirubicin each decreased growth of the Dst1:Rpb9 strain relative to the control; however, idarubicin did not specifically inhibit this strain relative to the control (Fig. 4*C*). Importantly, Dst1:Rpb9-specific chemical sensitivity was not observed in the absence of MTX selection (Fig. S2*A*), suggesting that the observed growth changes are indeed the result of changes in cellular levels of the Dst1:Rpb9 complex.

Similar to their effects on Dst1:Rpb9, doxorubicin, daunorubicin, and epirubicin each induced haploinsufficiency of *SSL2*, whereas idarubicin did not (Fig. 4*D*). These results identify the 4-methoxy group (which is absent in idarubicin) as critical for the effects on both the Dst1:Rpb9 complex and *SSL2* haploinsufficiency. This structure-activity relationship is perhaps surprising given that all four drugs are DNA intercalators, as illustrated by the sensitivity of the *rad55*Δ and *rad57*Δ homozygous yeast deletion strains (Fig. 4*E*). Given their widespread and overlapping clinical applications, further investigation of these differences in yeast and humans is certainly warranted. We note that doxorubicin-dependent depletion of Dst1:Rpb9 cannot be explained by down-regulation of either gene (Fig. S2*B*), but whether doxorubicin disrupts this interaction directly remains to be determined.

Specific Depletion of the Cit2:Cit2 Complex by Multiple Chemical Compounds. The remaining four high-confidence chemical-PPI pairs in which a strain exhibited specific sensitivity in our pool assay, each involved the Cit2:Cit2 strain. This strain was found to be sensitive to four compounds when grown under MTX selection: haematommic acid ethyl ester, cbf_5236571, chaulmoogric acid, and methyl 7-deshydroxypyrogallin-4-carboxylate (Fig. S3*A*). *CIT2* encodes the peroxisomal citrate synthase that catalyzes the condensation of acetyl CoA and oxaloacetate to form citrate (28). Reduced growth of the isogenic Cit2:Cit2 strain in response to each compound was verified to be dependent on MTX selection (Fig. S3 *B* and *C*). Examination of *CIT2* transcript levels revealed a significant decrease in response to each of these chemical compounds (Fig. S3*D*), suggesting that the observed reduction in the Cit2:Cit2 complex is perhaps best explained by reduced transcript levels and thus Cit2 abundance. The origin and potential benefits of this cellular adaptation to chemical stress remain unknown.

Chemical-Induced Accumulation of Multidrug Transporter Complexes. Instances of chemical-induced growth increases identified by our screens overwhelmingly involved strains representing multidrug transporter complexes, specifically, Pdr5:Pdr5, Snq2:Snq2, and Tpo1:Pdr5 (Fig. 3*A*). We examined whether these three strains responded differently to the 80 chemical compounds tested. Hierarchical clustering of the interaction scores for these three strains identified three distinct clusters of compounds (Fig. 5*A*

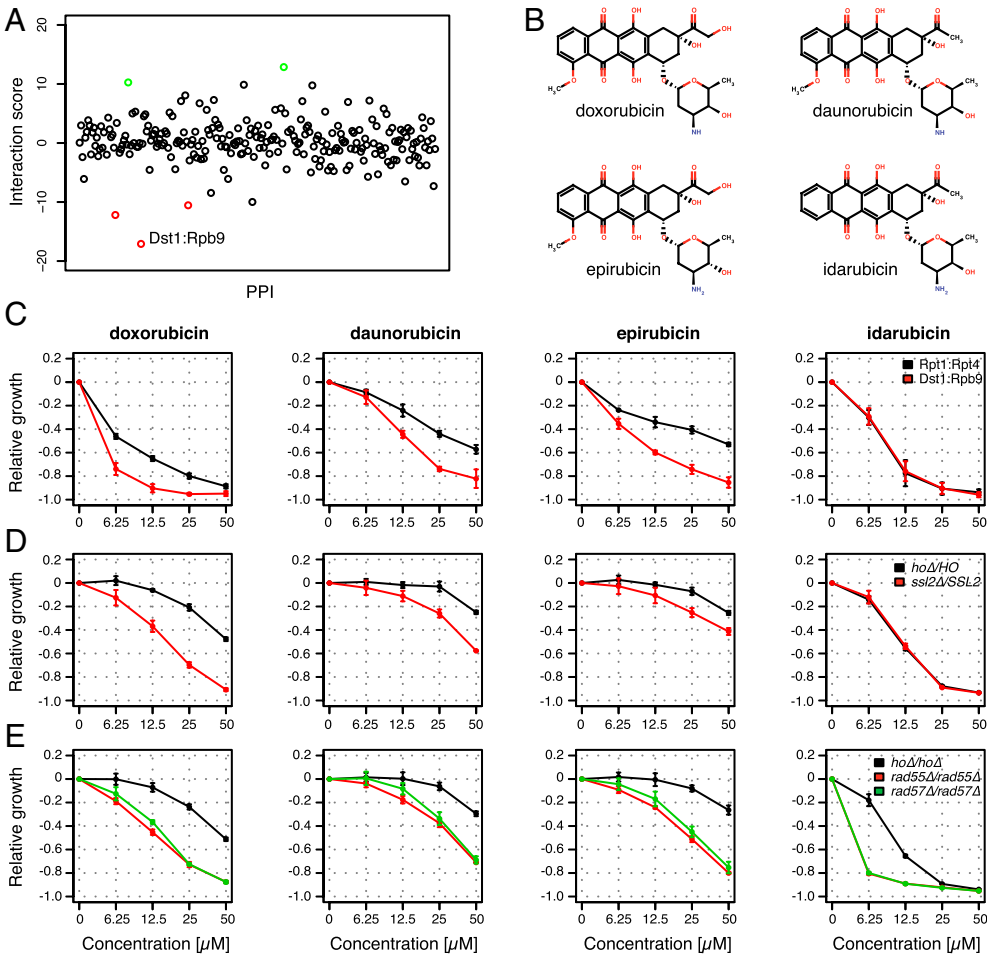

Fig. 4. Specific depletion of the Dst1:Rpb9 complex by doxorubicin, but not by idarubicin. (*A*) Dot plot depicting the interaction scores of 238 PPIs assayed in 12.5 μM doxorubicin. PPIs with scores less than −10 are depicted in red and those with scores greater than10 in green. Dst1:Rpb9, the most sensitive strain in this condition, is labeled. (*B*) Molecular structures of doxorubicin, daunorubicin, epirubicin, and idarubicin. (*C*) Confirmation of pool data with isogenic cultures. Dst1:Rpb9 and Rpt1:Rpt4 (control) were grown under MTX selection and in increasing concentrations of doxorubicin, daunorubicin, epirubicin, or idarubicin (concentrations are indicated on the *x* axis of each plot). Growth relative to that in the absence of drug is indicated by the *y* axis. The mean of four independent replicates is plotted. Error bars represent the SD. (*D*) Growth in rich media (yeast extract/peptone/dextrose broth) of the *hoΔ/HO* (control) and *ssl2Δ/SSL2* heterozygous deletion strains in the presence of increasing concentrations of doxorubicin, daunorubicin, epirubicin, or idarubicin. Growth relative to that in the absence of drug is indicated by the *y* axis, and drug concentration on the *x* axis. The mean of three independent replicates is plotted. Error bars represent the SD. (*E*) As in *D*, but involving the *hoΔ/hoΔ*, *rad55Δ/rad55Δ*, and *rad57Δ/rad57Δ* homozygous deletion strains.

and Fig. S4). The first cluster contained compounds that enhanced growth of all three strains, but especially the Pdr5:Pdr5 strain. Compounds in the second cluster weakly enhanced the three strains, but showed no preference for Pdr5:Pdr5. In contrast, the third cluster contained compounds that specifically enhanced growth of the Snq2:Snq2 strain. We verified the specificity for Snq2:Snq2 for one chemical in this cluster (cbf_5236571) using isogenic cultures (Fig. S5*A*). These findings demonstrate that the cell's response to different chemical insults is complex and mediated through different ABC transporters, as noted previously (29).

It has been previously demonstrated that transcript levels of *SNQ2* and *PDR5* are induced several fold in response to FK506 (30). Indeed, we observed that FK506-enhanced growth of the Tpo1:Pdr5 strain was dependent on Pdr1 (Fig. S5*B*), a transcription factor that controls the expression of many multidrug resistance genes (31, 32). We therefore reasoned that the accumulation of binary pump complexes could be due, at least in part, to transcriptional up-regulation of the corresponding genes. We confirmed this with quantitative RT-PCR and found a strong induction of *PDR5* and a moderate activation of the *SNQ2* and *TPO1* genes in response to FK506 (Fig. 5*B*). Similarly, transcript levels of *SNQ2* were strongly induced following exposure to cbf_5236571, whereas expression of both *PDR5* and *TPO1* did not change greatly (Fig. 5*B*).

To further explore the drug response in yeast, we used a simple growth assay to measure abundance changes of the Tpo1:Pdr5 and Snq2:Pdr5 binary complexes in response to 1,246 unique chemical compounds (Dataset S4). In total, 388 compounds (~31% of those tested) strongly enhanced growth of the Tpo1:Pdr5 and/or the Snq2:Pdr5 strains. We examined this group of molecules (hereafter referred to as active compounds) for shared properties and found that nitrogen-containing compounds were significantly less likely to be among the active set (χ^2-test, $P = 8.09 * 10^{-18}$). We also found the lipophilicity (LogP) of actives to be significantly higher (mean LogP = 3.15) than the remaining compounds (mean LogP = 1.72) ($P = 1.22 * 10^{-22}$; Fig. 5*C*). These results expand previous work demonstrating induction of drug pumps by membrane-active compounds (33). Active compounds also tended to have fewer hydrogen bond acceptors and donors compared with inactive compounds; however, the molecular weight of active and inactive compounds did not differ significantly (Fig. 5*C*).

Discussion

In the present study, a robust cell-based assay was developed by applying molecular barcoding to the mDHFR PCA system and

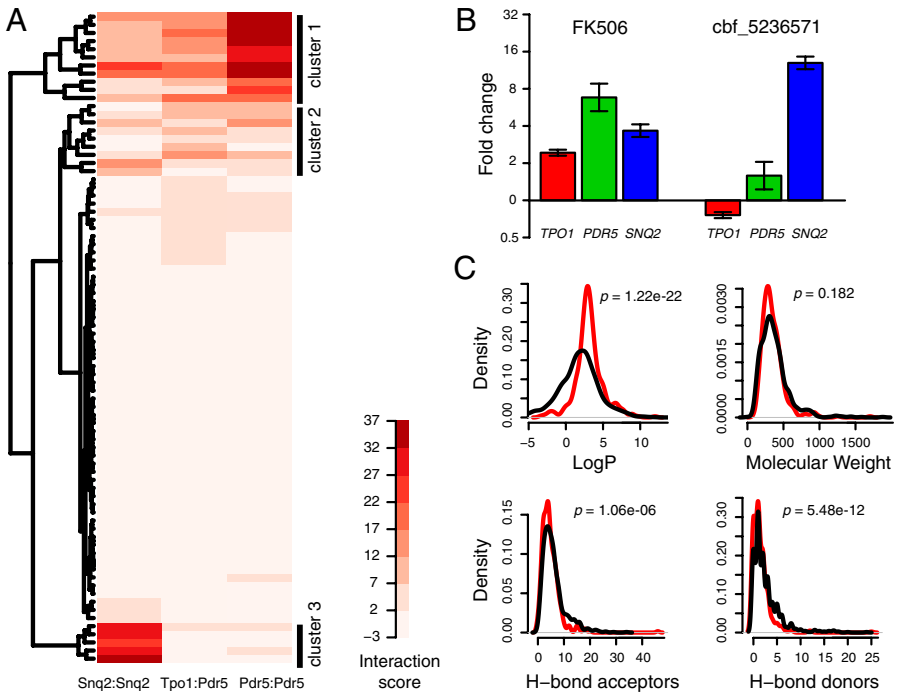

Fig. 5. Assessing the multidrug response in yeast using PCA. (*A*) Heat map and dendrogram depicting the results of hierarchical clustering of interaction scores for Pdr5:Pdr5, Snq2:Snq2, and Tpo1:Pdr5. Darker shades of red indicate higher interaction scores and therefore a greater increase in complex abundance ("Interaction score"). (*B*) Bar plot showing changes in *TPO1*, *PDR5*, and *SNQ2* transcript levels (indicated in red, green, and blue, respectively) in cells treated with 50 μM FK506 (*Left*) or 50 μM cbf_5236571 (*Right*) for 1 h. Fold change relative to a "no drug" control is plotted on the *y* axis. Data were normalized using *ACT1* as a control. The mean of three independent replicates is plotted. Error bars represent the SD. (*C*) Distribution plot of LogP (*Upper Left*), molecular weight (*Upper Right*), hydrogen bond acceptors (*Lower Left*), and hydrogen bond donors (*Lower Right*) for "active" chemical compounds (those that enhance growth of the Tpo1:Pdr5 and/or the Snq2:Pdr5 strains) and for "non-active" compounds, shown as red and black curves, respectively. In each panel, the Wilcoxon rank-sum test was used to determine whether the distribution of active and nonactive compounds was significantly different. *P* values are reported at the upper right of each panel.

thus allowing parallel analysis of protein–protein complexes in their natural cellular environment. We applied this assay to measure changes (both positive and negative) in 238 binary protein complexes in response to 80 unique chemical entities. With few exceptions, these 80 chemicals were not preselected on the basis of biological activity in yeast; however, 14 inhibited growth of a wild-type strain in the absence of MTX selection (Dataset S1). In total, 22 of the 80 chemicals that we tested induced a change in at least one binary complex, the majority of which involved drug-efflux pumps (Fig. 3*A*). Poor cell permeability can be an obstacle of cell-based assays in yeast, whose cell wall and elaborate chemical defense mechanisms represent a formidable barrier to many chemical compounds. Although it is unclear how many compounds were actually able to penetrate into yeast, prescreening compounds for growth inhibition of a wild-type strain, applying computational models to prioritize cell-permeable bioactive compounds (34), or genetically disabling yeast's chemical defense mechanisms (35, 36) could each increase the number of compounds effectively entering the cell in future studies. Indeed, in the current study our "hit rate" was much higher for growth inhibitory compounds, as 13 of the 14 growth inhibitors identified at least one change in our multiplex assay.

Our approach readily identified the previously described disruption of Hom3:Fpr1 by FK506 (19) (Fig. 3 *C* and *D*). This observation confirms that the mDHFR-based PCA system is reversible. Even though this had been aptly demonstrated in vitro (8), it was important to verify in vivo, given the irreversibility of other, specifically, popular fluorescent protein-based PCAs (37). This result also demonstrates that disruption of a single PPI can be easily detected in a pool of strains representing hundreds of unique PPIs.

Among the chemical-dependent changes that we identified was the reduced abundance of the Dst1:Rpb9 complex in the presence of doxorubicin, a founding member of the anthracycline class of chemotherapeutic drugs (38). Despite their longstanding and widespread clinical use, the therapeutic mechanism of action of anthracyclines remains ill-defined. Inhibition of topoisomerase II is often regarded as the basis of anthracyclines' potent anti-tumor effects; however, experimental evidence supports other mechanisms as well (39). Recent work has identified Ssl2 as the likely target of doxorubicin in yeast that is rate-limiting for growth (24, 25). Doxorubicin's effect on Dst1:Rpb9 (Fig. 4 *A* and *C*) is especially noteworthy, given the functional relationship between Ssl2 (a component of the RNA polymerase transcription factor TFIIH) and these two proteins: Dst1 is a transcription elongation factor for RNA Pol II and Rpb9 is a subunit of RNA Pol II required for transcription start-site selection (20, 21, 40, 41). These functional links, in addition to the similar structure-activity relationships that we observed (Fig. 4 *B–D*), strongly suggest that *SSL2* haploinsufficiency and cellular depletion of the Dst1:Rpb9 complex are interdependent somehow. Our results point to a mechanism for doxorubicin-mediated growth inhibition that may involve transcription start-site selection, transcript elongation through arrest sites, or both.

Multidrug resistance continues to be a major obstacle in effectively treating many cancers (42). The utility of yeast as a model for studying multidrug resistance is supported by its vast repertoire of drug transporters (29, 35) and by the homology of both Pdr5 and Snq2 to human Mdr1, a major contributor to tumor resistance (43, 44). Of the 80 chemicals screened in this study, 21 (26.25%) yielded an interaction score >10 in at least one of three drug-pump strains (Pdr5:Pdr5, Snq2:Snq2, or Tpo1:Pdr5). We took advantage of this phenomenon to assess the yeast drug response in ~1,250 unique chemical compounds using a simple growth assay. The observation that elevated chemical lipophilicity significantly correlates with accumulation of binary pump complexes confirms on a broad level earlier studies that were based on a small number of chemicals (33). Extending these assays to larger numbers of small molecules could lead to

a better understanding of the chemical features that trigger the multidrug response in yeast or even to predictive models that could aid in designing more effective therapeutics.

The highly multiplexed nature of our assay allows for the interrogation of many binary protein complexes in a single experiment. The pool of ~250 strains described here can easily be increased in complexity to interrogate more PPIs. Furthermore, this approach is not limited to yeast proteins, but can also be adapted for studying interactions between proteins from higher eukaryotes (1–4). Our current results suggest that additional screens involving more complex pools will reveal the dynamic nature of the cell's interactome, provide valuable mechanistic information for bioactive compounds, and extend our understanding of PPI druggability.

Materials and Methods

Media and Growth Conditions. PCA-PPI harboring strains were selected in minimal media supplemented with 100 μg/mL MTX. Isogenic cultures (100 μL) were inoculated at a concentration of 0.01 OD_{600}/mL and grown in 96-well microtiter plates at 30 °C. Optical density was measured every 15 min over the course of several hours (as indicated in graphs) using a GENios microplate reader (Tecan). Area under the curve (AUC) was used to assess growth, a detailed description of which is in *SI Materials and Methods*.

PCA Pool Construction and Screening. The Yeast Interactome Collection (YSC5849) from Open Biosystems was used to construct a pool of barcoded mDHFR-tagged strains (described in *SI Materials and Methods*). Frozen aliquots of the pool were recovered in minimal media and then diluted in minimal media plus MTX. Cells were then grown in the presence of chemical compound or DMSO in 700-μL cultures in a 48-well microplate. The screening concentrations of all compounds tested are listed in Dataset S1. After five generations of growth, cells were harvested, and genomic DNA was extracted. PCR amplification of barcodes and hybridization to Genflex Tag 16k arrays (Affymetrix) were performed as described previously (45). Raw data are available via EBI's ArrayExpress archive (accession no. E-MEXP-3467). Data analysis and the calculation of "interaction scores" for each chemical-PPI pair are described in *SI Materials and Methods*.

Quantitative RT-PCR Experiments. Total RNA was extracted from strain BY4743 growing in minimal media in the presence of compound or DMSO (control) using the RiboPure-Yeast kit (Ambion). RNA was reverse-transcribed into cDNA using SuperScript II (Invitrogen) and oligo(dT)12–18 primer (Invitrogen). Data analysis and the calculation of fold changes of transcript levels in response to drug treatment are described in *SI Materials and Methods*.

ACKNOWLEDGMENTS. We thank Stephen Michnick for advice on experiments and helpful comments on the manuscript. We also thank Julia Oh for providing reagents, Patrick Flaherty for helpful discussion, and Michael Proctor and Ana Maria Aparicio for technical assistance. This research was funded by Grant R21HG005785-01 from the National Human Genome Research Institute to R.W.D. and R.P.S.

1. Rual JF, et al. (2005) Towards a proteome-scale map of the human protein-protein interaction network. *Nature* 437:1173–1178.
2. Stelzl U, et al. (2005) A human protein-protein interaction network: A resource for annotating the proteome. *Cell* 122:957–968.
3. Giot L, et al. (2003) A protein interaction map of Drosophila melanogaster. *Science* 302:1727–1736.
4. Li S, et al. (2004) A map of the interactome network of the metazoan C. elegans. *Science* 303:540–543.
5. Yu H, et al. (2008) High-quality binary protein interaction map of the yeast interactome network. *Science* 322:104–110.
6. Uetz P, et al. (2000) A comprehensive analysis of protein-protein interactions in Saccharomyces cerevisiae. *Nature* 403:623–627.
7. Ito T, et al. (2000) Toward a protein-protein interaction map of the budding yeast: A comprehensive system to examine two-hybrid interactions in all possible combinations between the yeast proteins. *Proc Natl Acad Sci USA* 97:1143–1147.
8. Tarassov K, et al. (2008) An in vivo map of the yeast protein interactome. *Science* 320: 1465–1470.
9. MacDonald ML, et al. (2006) Identifying off-target effects and hidden phenotypes of drugs in human cells. *Nat Chem Biol* 2:329–337.
10. Arkin MR, Wells JA (2004) Small-molecule inhibitors of protein-protein interactions: Progressing towards the dream. *Nat Rev Drug Discov* 3:301–317.
11. Pagliaro L, et al. (2004) Emerging classes of protein-protein interaction inhibitors and new tools for their development. *Curr Opin Chem Biol* 8:442–449.
12. Mullard A (2012) Protein-protein interaction inhibitors get into the groove. *Nat Rev Drug Discov* 11:173–175.
13. Michnick SW, Ear PH, Manderson EN, Remy I, Stefan E (2007) Universal strategies in research and drug discovery based on protein-fragment complementation assays. *Nat Rev Drug Discov* 6:569–582.
14. Giaever G, et al. (2004) Chemogenomic profiling: Identifying the functional interactions of small molecules in yeast. *Proc Natl Acad Sci USA* 101:793–798.
15. Giaever G, et al. (1999) Genomic profiling of drug sensitivities via induced haploinsufficiency. *Nat Genet* 21:278–283.
16. Lum PY, et al. (2004) Discovering modes of action for therapeutic compounds using a genome-wide screen of yeast heterozygotes. *Cell* 116:121–137.
17. Remy I, Michnick SW (1999) Clonal selection and in vivo quantitation of protein interactions with protein-fragment complementation assays. *Proc Natl Acad Sci USA* 96: 5394–5399.
18. Pelletier JN, Arndt KM, Plückthun A, Michnick SW (1999) An in vivo library-versus-library selection of optimized protein-protein interactions. *Nat Biotechnol* 17:683–690.
19. Alarcón CM, Heitman J (1997) FKBP12 physically and functionally interacts with aspartokinase in Saccharomyces cerevisiae. *Mol Cell Biol* 17:5968–5975.
20. Cramer P (2002) Multisubunit RNA polymerases. *Curr Opin Struct Biol* 12:89–97.
21. Ubukata T, Shimizu T, Adachi N, Sekimizu K, Nakanishi T (2003) Cleavage, but not read-through, stimulation activity is responsible for three biologic functions of transcription elongation factor S-II. *J Biol Chem* 278:8580–8585.
22. Momparler RL, Karon M, Siegel SE, Avila F (1976) Effect of adriamycin on DNA, RNA, and protein synthesis in cell-free systems and intact cells. *Cancer Res* 36:2891–2895.
23. Fornari FA, Randolph JK, Yalowich JC, Ritke MK, Gewirtz DA (1994) Interference by doxorubicin with DNA unwinding in MCF-7 breast tumor cells. *Mol Pharmacol* 45:649–656.
24. Furuchi T, Nitta K, Takahashi T, Naganuma A (2004) Overexpression of Ssl2p confers resistance to adriamycin and actinomycin D in Saccharomyces cerevisiae. *Biochem Biophys Res Commun* 314:844–848.
25. Smith AM, et al. (2009) Quantitative phenotyping via deep barcode sequencing. *Genome Res* 19:1836–1842.
26. Sung P, Guzder SN, Prakash L, Prakash S (1996) Reconstitution of TFIIH and requirement of its DNA helicase subunits, Rad3 and Rad25, in the incision step of nucleotide excision repair. *J Biol Chem* 271:10821–10826.
27. Tirode F, Busso D, Coin F, Egly JM (1999) Reconstitution of the transcription factor TFIIH: Assignment of functions for the three enzymatic subunits, XPB, XPD, and cdk7. *Mol Cell* 3:87–95.
28. Lewin AS, Hines V, Small GM (1990) Citrate synthase encoded by the CIT2 gene of Saccharomyces cerevisiae is peroxisomal. *Mol Cell Biol* 10:1399–1405.
29. Rogers B, et al. (2001) The pleitropic drug ABC transporters from Saccharomyces cerevisiae. *J Mol Microbiol Biotechnol* 3:207–214.
30. Marton MJ, et al. (1998) Drug target validation and identification of secondary drug target effects using DNA microarrays. *Nat Med* 4:1293–1301.
31. Balzi E, Wang M, Leterme S, Van Dyck L, Goffeau A (1994) PDR5, a novel yeast multidrug resistance conferring transporter controlled by the transcription regulator PDR1. *J Biol Chem* 269:2206–2214.
32. Katzmann DJ, Hallstrom TC, Mahé Y, Moye-Rowley WS (1996) Multiple Pdr1p/Pdr3p binding sites are essential for normal expression of the ATP binding cassette transporter protein-encoding gene PDR5. *J Biol Chem* 271:23049–23054.
33. Schüller C, et al. (2007) Membrane-active compounds activate the transcription factors Pdr1 and Pdr3 connecting pleiotropic drug resistance and membrane lipid homeostasis in Saccharomyces cerevisiae. *Mol Biol Cell* 18:4932–4944.
34. Wallace IM, et al. (2011) Compound prioritization methods increase rates of chemical probe discovery in model organisms. *Chem Biol* 18:1273–1283.
35. Suzuki Y, et al. (2011) Knocking out multigene redundancies via cycles of sexual assortment and fluorescence selection. *Nat Methods* 8:159–164.
36. Decottignies A, et al. (1998) ATPase and multidrug transport activities of the overexpressed yeast ABC protein Yor1p. *J Biol Chem* 273:12612–12622.
37. Magliery TJ, et al. (2005) Detecting protein-protein interactions with a green fluorescent protein fragment reassembly trap: Scope and mechanism. *J Am Chem Soc* 127:146–157.
38. Minotti G, Menna P, Salvatorelli E, Cairo G, Gianni L (2004) Anthracyclines: Molecular advances and pharmacologic developments in antitumor activity and cardiotoxicity. *Pharmacol Rev* 56:185–229.
39. Gewirtz DA (1999) A critical evaluation of the mechanisms of action proposed for the antitumor effects of the anthracycline antibiotics adriamycin and daunorubicin. *Biochem Pharmacol* 57:727–741.
40. Goel S, Krishnamurthy S, Hampsey M (2012) Mechanism of start site selection by RNA polymerase II: Interplay between TFIIB and Ssl2/XPB helicase subunit of TFIIH. *J Biol Chem* 287:557–567.
41. Sun ZW, Tessmer A, Hampsey M (1996) Functional interaction between TFIIB and the Rpb9 (Ssu73) subunit of RNA polymerase II in Saccharomyces cerevisiae. *Nucleic Acids Res* 24:2560–2566.
42. Gottesman MM, Fojo T, Bates SE (2002) Multidrug resistance in cancer: Role of ATP-dependent transporters. *Nat Rev Cancer* 2:48–58.
43. Sipos G, Kuchler K (2006) Fungal ATP-binding cassette (ABC) transporters in drug resistance and detoxification. *Curr Drug Targets* 7:471–481.
44. Kuchler K, Thorner J (1992) Functional expression of human mdr1 in the yeast Saccharomyces cerevisiae. *Proc Natl Acad Sci USA* 89:2302–2306.
45. Giaever G, et al. (2002) Functional profiling of the Saccharomyces cerevisiae genome. *Nature* 418:387–391.